ISSN 1028-334X, Doklady Earth Sciences, 2024, Vol. 515, Part 1, pp. 423–429. © Pleiades Publishing, Ltd., 2024.
ISSN 1028-334X, Doklady Earth Sciences, 2024. © Pleiades Publishing, Ltd., 2024.

PETROLOGY

Estimation of Chlorine Fugacity in Low-H_2O Fluid of the C–O–(H)–NaCl System in the Cumulus of Ultramafic–Mafic Intrusions

A. G. Simakin[a,*], O. Yu. Shaposhnikova[a], V. N. Devyatova[a], S. I. Isaenko[b], and D. D. Eremin[c]

Presented by Academician L.Ya. Aranovich November 20, 2023

Received November 20, 2023; revised November 29, 2023; accepted November 30, 2023

Abstract—At high *PT* parameters of cumulates of ultramafic–mafic intrusions and low oxygen fugacity (below QFM buffer), Pt in the form of a carbonyl complex is dissolved in a CO_2-bearing fluid. The high solubility of Pt chloride in brines with NaCl, which is related to the formation of low-sulfide deposits of platinum group elements, is attained only at high oxygen fugacity (above the QFM buffer). It is suggested that native platinum at low oxygen fugacity in low-H_2O CO–CO_2 (H_2O) fluid can also transit into a cation-soluble form due to the reaction of chloration. The experimental data are provided for the interaction of NaCl with magnetite and chromite (accessory minerals of ultramafic–mafic intrusions) at P = 200 MPa, T = 950°C, and fO_2 <QFM with the formation of Fe and Cr chlorides. As shown by thermodynamic calculations, the $FeCl_3$ and $FeCl_2$ equilibrium provides a high chlorine fugacity (fCl_2), which is only 3–4 orders of magnitude lower than fCl_2 in Pt–$PtCl_2$ equilibrium and 2.5–3.0 orders of magnitude higher than in 1 M HCl aqueous fluid at the same P–T–fO_2 parameters.

Keywords: platinum, ultramafic–mafic intrusives, fluid, experiment, chlorine fugacity

DOI: 10.1134/S1028334X23603292

INTRODUCTION

Low-sulfide deposits of platinum group elements (PGEs) form during late magmatic and early postmagmatic processes in ultramafic–mafic intrusives as a result of fluid transport. In some cases, it has been established that the fluid transport is not related to the cooling of a host intrusive (Konder), but is delayed for millions and tens of millions of years [1]. To create a physicochemical model of ore formation, it is important to identify the composition of the fluid and *PT* and redox parameters responsible for the PGE solubility. The increasing solubility enhances the potential volume of a redeposited metal and the scale of ore mineralization.

Chlorine achieves special attention upon the formation of low-sulfide PGE deposits [2]. In fact, the solubility of platinum and gold is high in Cl-bearing environments (fluid, Cl brine) at high oxygen fugacity [3, 4]. At high *PT* parameters of the intrusive cumulus and low oxygen fugacity near QFM/QFM-2 = CCO, native platinum forms stable carbonyl complexes in the fluid phase [5].

According to modern experimental data [6] on the solubility of Pt in a brine at $P \approx 200$ MPa and T = 900–950°C, the slope of the solubility–fO_2 correlation in log–log coordinates is ~1/2. Extrapolation of data to low oxygen fugacity corresponding to the CCO (QFM-2) buffer yields the estimated solubility of 0.5–1.0 ppm in the brine, which is more than two orders of magnitude lower than the carbonyl solubility.

Platinum can theoretically be transferred to chloride also at low fO_2 due to the relatively high chlorine fugacity. In this case, the presence of CO provides for the formation of a mixed carbonyl–chloride Pt complex with a higher fugacity ($PtCl_2(CO)_2$). Its high fugacity was suggested to apply for etching of Pt films using a CO/Cl_2 gas mixture with a mole ratio of 2/1 [7]. The authors of [8] calculated the composition of low-H_2O (an H_2O content of no more than 10 mol %) fluid in the C–O–H–Cl system and predicted a high amount (~1/2) of Cl_2 and $COCl_2$ from the total

[a] *Korzhinskii Institute of Experimental Mineralogy, Russian Academy of Sciences, Chernogolovka, Moscow oblast, 142432 Russia*

[b] *Yushkin Institute of Geology, Komi Science Center, Ural Branch, Russian Academy of Sciences, Syktyvkar, 167982 Russia*

[c] *Moscow State University, Moscow, 119991 Russia*

**e-mail: simakin@iem.ac.ru*

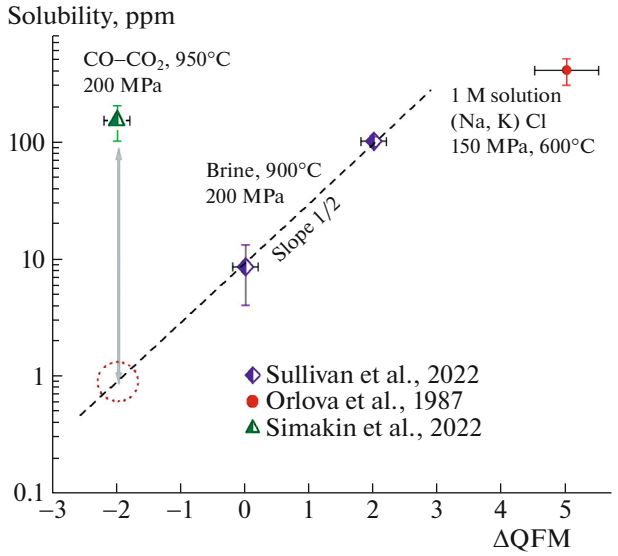

Fig. 1. Experimental data on Pt solubility in the fluid at high temperature depending on the oxygen fugacity. The dotted circle shows the solubility in brine at low oxygen fugacity, which was extrapolated according to [6].

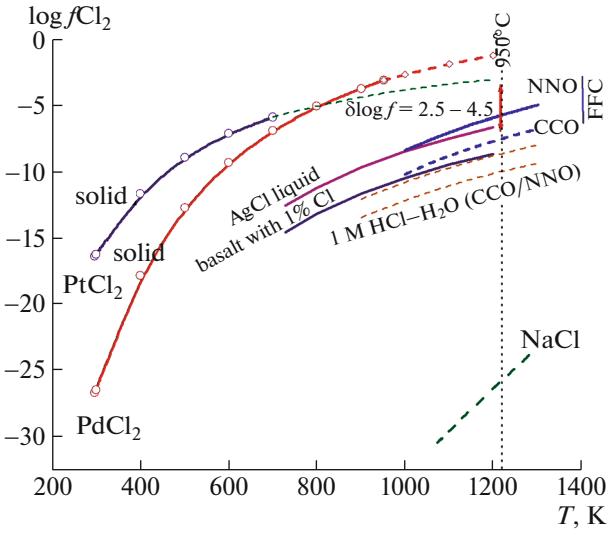

Fig. 2. Chlorine fugacities equilibrated in metal–chloride couple, which are calculated using the thermodynamic database [9]. Data for $PtCl_2$ and $PdCl_2$ are extrapolated to high T (dotted line). The chlorine fugacity, which provides the Cl content of ~1 wt % in dry basaltic melt at 1400°C [10], is shown separately. Chlorine fugacities corresponding to $FeCl_3$–$FeCl_2$ equilibria (FFC) at oxygen fugacities of NNO and CCO are also shown. Chlorine fugacities in 1 M HCl aqueous fluid (P = 200 MPa) calculated by the reaction $2HCl + 1/2O_2 = H_2O + Cl_2$ at two oxygen fugacities (CCO and NNO buffers) are also shown.

Cl content accepted as 5 mol %. At a total pressure accepted in the calculations as 300 MPa, this content corresponds to the chlorine fugacity of >10 bar.

Figure 2 shows the chlorine fugacity in the Pd–$PdCl_2$ and Pt–$PtCl_2$ equilibria, which are calculated using thermodynamic data from [9], and at T = 950°C the equilibrium fugacity is much lower than 1 bar and is 0.1 and 0.001 bar, respectively. With fluid of the composition calculated in [8], Pd and Pt react with the formation of chlorides. At the same time, the chlorine fugacity can be buffered by cumulus minerals. The Ag and AgCl–AgI mixture couple is used in experiments with low-H_2O (nominally H_2O-free) melts as a buffer of chlorine fugacity [10]. Pure Ag chloride yields too high a chlorine fugacity, which leads to the separation of Ca, Mg, and other cation chloride melt upon the reaction with the basaltic melt. NaCl is the most abundant Cl form at a low-temperature stage of the evolution of the ultramafic–mafic intrusions (see review in [11]). It can be suggested that, as a result of exchange reactions of NaCl with phases, which contain transitional metals of varying valency (Fe, Cr, Mn), the high temperature and the presence of low-H_2O fluid can lead to the formation of chlorides, which buffer the chlorine fugacity as a result of the following reaction:

$$MeCl_3 = MeCl_2 + 1/2Cl_2. \quad (1)$$

The proportion of two- and three-valence metal chlorides is related to oxygen fugacity, the value of which in turn is also buffered by cumulus minerals and the fluid (e.g., CCO buffer in the presence of CO_2 and graphite).

The first aim of the experimental study of the influence of chlorine on the PGE solubility in the low-H_2O fluid at low oxygen fugacity is a transition from low-active NaCl in the initial system to chlorides of transitional metals, which can provide a high chlorine fugacity. In this work, we present the results of experimental study of the reaction of this reduced fluid with NaCl and minerals of the spinel series at the parameters of the cumulus of ultramafic–mafic intrusions (P = 200 MPa and T = 950°C) and thermodynamic estimations of fCl_2 in this system.

METHODS

Initial Materials

This run series is the initial stage of study of the PGE solubility in Cl-bearing low-H_2O fluid, which used a wide spectrum of substances to search for the optimal conditions. Natural magnesite from South Urals, which was kindly provided by the Fersman Mineralogical Museum, Russian Academy of Sciences (FMM RAS, Moscow, Russia), was used as a CO_2 source. The composition of magnesite was determined on an electron microprobe and an inductively coupled plasma mass spectrometer (ICP-MS) at the Institute of Microelectronic Technology Problems (Chernogolovka, Russia). Siderite was used as the CO source: monomineral $FeCO_3$ (10 mol % $MnCO_3$) and

natural siderite from the FMM RAS. The decomposition of siderite and full reaction of wüstite with CO_2 leads to the formation of a CO and CO_2 mixture with a mole ratio of 1 : 2.

$$\begin{aligned} FeCO_3 &= FeO + CO_2, \\ 3FeO + CO_2 &= Fe_3O_4 + CO. \end{aligned} \quad (2)$$

We also used Mg oxalate, the thermal decomposition of which produces an equimolar CO and CO_2 mixture:

$$\begin{aligned} MgC_2O_4 &= MgCO_3 + CO, \\ MgCO_3 &= MgO + CO_2. \end{aligned} \quad (3)$$

The initial oxalate is a crystal hydrate $MgC_2O_4 \cdot 2H_2O$. To remove water, it was annealed at $T = 275$°C for 3–4 h. The residual H_2O content of the fluid source was 0.4–0.5 wt % according to Karl–Fischer titration (KFT) measurements. In the case of using of pure oxalate, the minimum mole H_2O content of the generated fluid was 0.02–0.03. NaCl was used as the initial Cl form. In runs with siderite, Fe was sourced from wüstite and magnetite and the products of the reaction of fluid generation. The runs with pure oxalate also involved magnetite (Kovdor massif) and chromite (Rai-Iz massif). The fluid traps included a sintered quartz glass powder, a sintered quartz–albite glass, an albite glass, and sintered quartz glass threads (which are used as a heat insulator).

EXPERIMENTAL

The experiments were conducted on an UVGD-10000 high gas pressure apparatus at the Institute of Experimental Mineralogy, Russian Academy of Sciences (IEM RAS, Chernogolovka, Russia). The vessel was made up of stainless steel; the working medium was Ar. The temperature was measured and regulated using a Pt–Rh thermocouple, and the gradient-free zone in the furnace was 40–50 mm long. The pressure was measured using a piezosensor accurate to 5%. The temperature and pressure were controlled with a precision of ±2.5°C and ±1%, respectively. Quenching was performed by switching of the furnace at an ongoing water cooling with a rate of 150°C/min. Experiments mainly followed the two-capsule method. The outer and inner capsules were composed of Pt, Pd, and Au. The substances for the generation of the fluid and NaCl were placed into a small open capsule, and the fluid traps were placed into an outer welded capsule. Oxygen fugacity was given by a CO/CO_2 ratio near the CCO buffer, and excessive CO was decomposed with the formation of C and organic matter. In the case of using siderite, the oxygen fugacity is close to the wüstite–magnetite buffer (close to the CCO buffer at $T =$ 950°C). The capsules were blown by Ar and welded. The run parameters are shown in Table 1S (Supplementary Material).

Analysis

The H_2O content of starting substances was measured using an AQUQ 40 KFT system equipped with a heating unit of solid phases. According to the calibration data, the precision of the measurements was 3 rel %. The chemical analyses and surface images of the starting substances and experimental samples were performed on a CamScan MV2300 scanning electron microscope and a Tescan Vega TS5130MM SEM equipped with an INCA Energy 450 energy-dispersive spectrometer (EDS) with an INCA Penta FET X3Si (Li) semiconducting detector. The analyses were conducted an accelerating voltage of 20 kV and a beam current on a Co sample of 0.1–0.2 nA. The least beam diameter was 0.2 μm for the point phase analysis; some glasses were analyzed using a rectangular scanning area up to 50–80 μm wide. The measurement results were processed in the INCA Energy 200 software.

Raman Spectroscopy

The Raman spectra of experimental samples were measured in two laboratories. At the IEM RAS, the measurements were conducted on a RM1000 spectrometer equipped with a CCD camera, a marginal filter, and a Leica microscope with an objective of 50×. The spectra were excited by a solid-state laser with diode pumping and a wavelength of 532 nm. The measurement parameters were as follows: a laser output power of 22 mV, a slit length of 50 μm, and an accumulation time of 5 × 10 s. The measurements at the Institute of Geology, Komi Science Center, Ural Branch, Russian Academy of Sciences (IG KSC UB RAS, Syktyvkar, Russia), were conducted on a LabRam HR800 high-precision Raman spectrometer (Horiba, Jobin Yvon) using an external Ar^+ laser (514.5 nm, power of 1.2 mW). The spectrometer was equipped with an Olympus BX41 microscope with an objective of 50×. The spectra were recorded in the range of 100–4000 cm^{-1} using a spectrometer grating of 600 lines/mm. The sizes of the confocal hole and the slit were 300 and 100 μm, respectively. The size of the analyzed region was ~5 μm. Each spectrum was a result of three accumulations 10 s long. The measurements were conducted at room temperature.

RESULTS

This work presents the results of study of oxide matrices and the products of (i) the decomposition of solid fluid sources and (ii) the reaction between the fluid with NaCl and these oxides, as well as magnetite and chromite. The composition of fluid traps allows the estimation of the fluid composition using a micro-Raman spectroscope (albite glass traps) and the content of noble metals in the fluid: Pt, Pd, and Au depending on using capsules (quartz and albite–

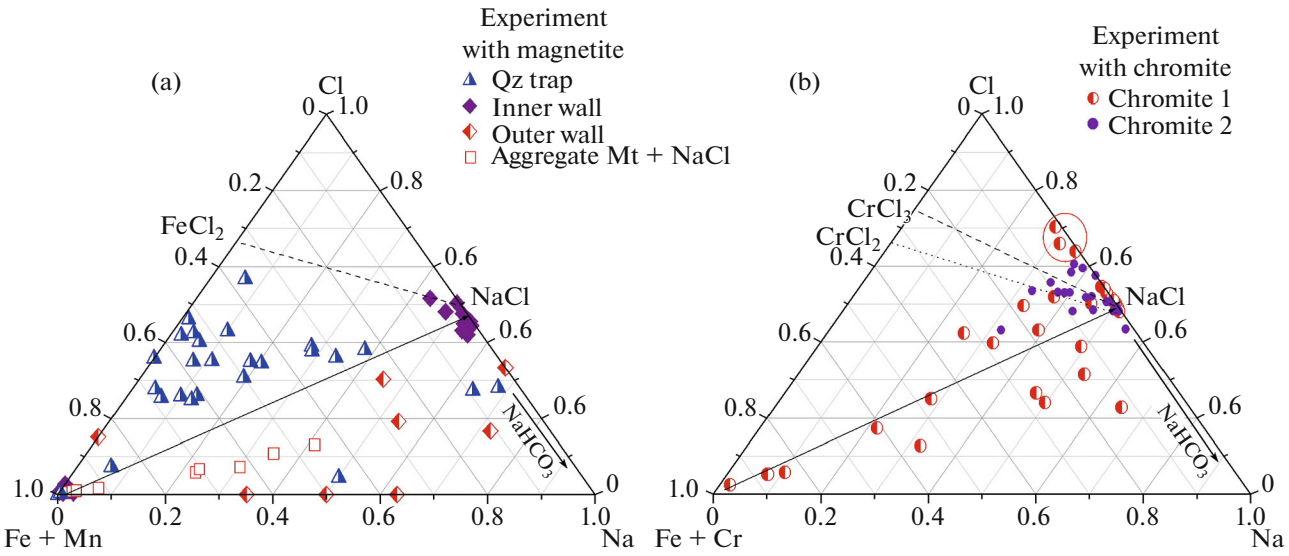

Fig. 3. Microprobe analyses (at %) of aggregates of small-disperse phases, which are the reaction products of generation of Cl-bearing fluid: (a) run O75, system with Fe on the walls of the inner and outer capsules, quartz trap, and magnetite; (b) two runs with chromite: first run with 10% NaCl and second run with 1% NaCl. The compositions inside the Fe(Cr)–NaCl–Na triangles reflect the presence of sodium Cl-free phases (Na_2CO_3, $NaHCO_3$, etc.). It is also evident from Fig. 3b that some compositions lie beyond the (Fe+Cr)–$CrCl_3$–NaCl triangle reflecting the presence of chlorides distinct from Na and Cr (+Fe) chlorides (probably Mg chlorides).

quartz glass traps). These data will be published in another work.

Results of Microprobe Analyses

The Fe and Mg oxides, which are the decomposition products of siderite, magnesite, and Mg oxalate are the main crystalline phases in the run products. The newly formed phases are small, thus preventing microprobe analysis of the composition of individual crystals. The analyses of phases from run O75 (a fluid source of siderite and oxalate; for details, see Table 1S, Supplementary Materials) are shown in the Fe–Na–Cl ternary diagram (at %) (Fig. 3). The Cl-free phases are unresolved on this diagram: Fe_3O_4, FeO(OH), FeO, $FeCO_3$, $NaHCO_3$, Na_2CO_3, and Fe oxy-chlorides. It is seen from Fig. 3 that some compositions correspond to a low-Fe area with a Na/Cl ratio of $\gg$1, which means the presence of Na salts formed as a result of exchange reactions of magnetite (wüstite) and NaCl (reaction 4, see below). Note also the absence of compositions with a Cl/Fe ratio of >2.0–2.2 possibly indicating the predominance of $FeCl_2$ in the composition of chlorides. As was mentioned above, $FeCl_3$ has a low boiling temperature (T_{boil}) and occurs in the fluid phase. In a similar (Fe + Cr)–Na–Cl diagram of the compositions of small-dispersed phases, numerous compositions of run products with chromite fall beyond the NaCl–$CrCl_2$ conode toward the high-Cl compositions in contrast to runs with magnetite. This can reflect the presence of a refractory crystalline $CrCl_3$ phase at the *PT* run parameters. Some compositions in the diagram occur on a NaCl–Cl segment of the Na–Cl side corresponding to the presence of $MgCl_2$, HCl or Cl-organic compounds.

Raman Spectroscopy Data

A Na carbonate, which is an important product of exchange reaction of spinels with NaCl, was found as $NaHCO_3$ only in the run with chromite and a high NaCl content. All the intense peaks coincide with the standard: k = 1268, 1047, and 686 cm^{-1}. The rare occurrence of $NaHCO_3$ in the experimental products, according to RMN spectroscopy, can be related to its high solubility in the fluid and its disperse precipitation upon quenching, as well as the formation of Na salts of organic acids.

The Fe chlorides, which form as a result of exchange reactions of NaCl with magnetite, were identified using Raman spectroscopy. Both $FeCl_3$ and, to a lesser extent, $FeCl_2$ are hygroscopic salts. Figure 4 shows a spectrum of partly decomposed siderite with weak bands of magnetite and evident bands k of 189 and 317 cm^{-1}. The Fe–Cl bond in a Fe dichloride crystal hydrate ($FeCl_2 \cdot 4H_2O$) is characterized by a band near 190 cm^{-1} [12]. Anhydrous $FeCl_2$ has a band at 152 cm^{-1} [13], which is identified in some spectra upon the decomposition together with a band at 187–190 cm^{-1}. Anhydrous $FeCl_3$ has the strongest line at 332 cm^{-1}. In hydrous solutions of $FeCl_3$, the strongest line at 315 cm^{-1} is attributed to Fe–Cl oscil-

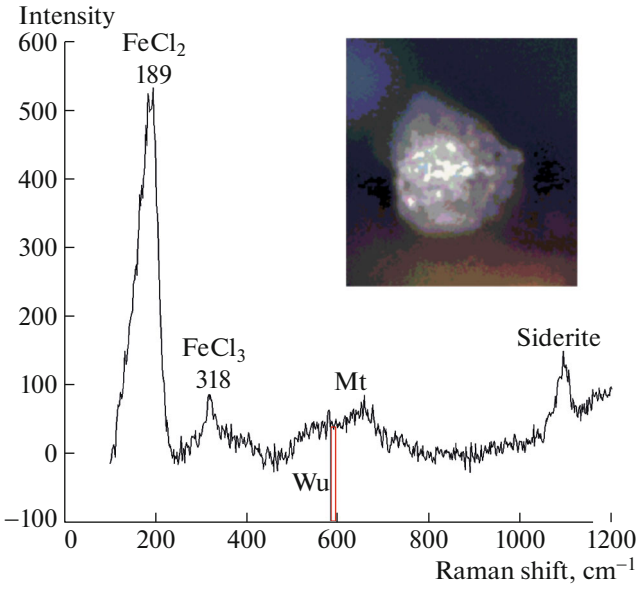

Fig. 4. Micro-Raman spectrum of reaction products of magnetite and NaCl in run O89 with a line of undecomposed siderite (fluid source) and merging wüstite and magnetite lines.

lations in the $FeCl_2^+$ complex [14]. The structural formula of crystal hydrates $FeCl_3$ is $[FeCl_2(H_2O)_4][FeCl_4] \cdot nH_2O$ ($n = 0..3$), i.e., they contain a structural unit $FeCl_2^+$ and are also identified by a line near 318 cm^{-1}. $FeCl_3$ is an extreme absorbent, the hydration of which could be triggered both by the fluid water and atmospheric water after the run.

In the reduced low-H_2O fluid, the runs yielded a weakly ordered carbon (the ratio of areas of D/G peaks in the Raman spectra is ~0.5) and a bitumen-like substance with a high luminescence (see the spectra in Supplementary Materials).

DISCUSSION AND CONCLUSIONS

Chemical Reactions in the Experiment

The experimental results showed that the reaction of NaCl in low-H_2O fluid with minerals of the spinel series results in the formation of transitional metal chlorides. These reactions can be written for the magnetite and magnochromite end-members:

$$6NaCl + Fe_3O_4 + 4CO = 3FeCl_2 + CO_2 + 3Na_2CO_3, \quad (4)$$

$$4NaCl + MgCr_2O_4 + 3CO = MgO + 2CrCl_2 + 2Na_2CO_3 + CO_2. \quad (5)$$

Reactions (4), (5) describe the formation of dichlorides. The formation of trichlorides can be described by the oxidation of dichlorides or the reaction of oxide phases with CO_2, e.g.,

$$3NaCl + 1/3Fe_3O_4 + 19/6CO_2 = FeCl_3 + 19/6CO + 3/2Na_2CO_3. \quad (6)$$

Soda, which is a product of reactions (4)–(6), was found as a hydrocarbonate by micro-Raman spectroscopy only in one run. The presence of Na salts distinct from NaCl is supported by bulk analysis of small-disperse run products close in composition to the Na–NaCl segment in the Na–(Fe + Cr)–Cl ternary diagram (Fig. 3). It can be suggested that the salts of organic acids (e.g., formic acid) form in the presence of a small H_2O content of the fluid:

$$2NaCl + FeO + 2CO + H_2O = FeCl_2 + 2NaCOOH. \quad (7)$$

The full thermodynamic calculation of reactions (4)–(6) requires refinement of which Na compounds form as a result of exchange reactions. As was discussed above, the equilibrium of $FeCl_2$–$FeCl_3$ and $CrCl_2$–$CrCl_3$ is buffered by chlorine fugacity as a result of the following reaction:

$$MeCl_3 = MeCl_2 + 1/2Cl_2. \quad (8)$$

It is important to take into account the phase state of chlorides at experimental *PT* conditions. $FeCl_3$ is a low-melting salt with a boiling temperature of 307°C present as a fluid component with varying fugacity, whereas $FeCl_2$ occurs as melt in equilibrium (8). The equilibrium $FeCl_3$ fugacity can be expressed as a function of oxygen fugacity in the presence of magnetite. Figure 2 shows the chlorine fugacity as a function of temperature at two oxygen fugacities. The chlorine fugacities in the Fe-bearing system are rather high and, at fO_2 = QFM-2, the chlorine fugacity (fCl_2) corresponds to fugacity, which provides the Cl content of ~1 wt % in the basaltic melt. At higher oxygen fugacity, it corresponds to the Ag–AgCl buffer and under magmatic conditions this fCl_2 triggers the formation of immiscible melts of Mg and Fe chlorides and a silicate liquid. These data are preliminary, first of all, because the $FeCl_2$ melt contains other chlorides.

$CrCl_3$ is a refractory compound with a melting temperature (T_{melt}) of 1152°C, whereas $CrCl_2$ is melting under experimental conditions but does not boil (T_{boil} = 1120°C); thus, the chlorine fugacity for a couple of pure Cr chlorides is fixed (Fig. 2) and approaches the Pt–$PtCl_2$ fugacity. The calculated oxygen fugacity in equilibrium with $MgCr_2O_4$ is close to QFM. As in the case with Fe chlorides, these calculations are also preliminary, because they ignore, first of all, the composition of the chloride melt. The exchange reaction $FeCl_2 + CrCl_3 = FeCl_3 + CrCl_2$ is also possible in the studied system, which is probably shifted to the right toward the formation of highly volatile chlorides. Note that $CrCl_3$ was identified on the Raman spectra of run products with chromite (Supplementary Material) in contrast to $CrCl_2$. The precise

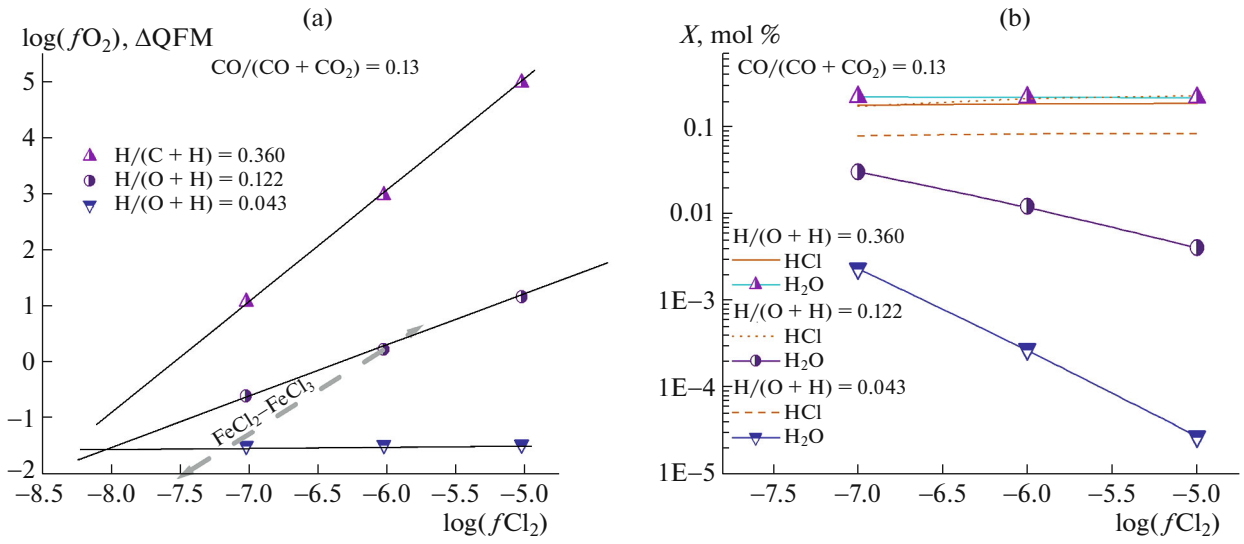

Fig. 5. Calculated according to reactions (9) in a low-water fluid C–O–H–Cl (the ratios $H/(O^{+}H) \sim X_{H_2O}$ are indicated on the graphs) (a) oxygen fugacity, the dotted line is the line corresponding to the $FeCl_2$–$FeCl_3$ buffer in the presence of magnetite at different f_{O_2}; (b) mole fractions of H_2O and HCl depending on $\log(XCl_2)$.

calculation of chlorine fugacity with chlorides is a difficult task requiring additional experimental data.

The presence of even a low H_2O content in the fluid leads to the predominance of HCl, which forms from molecular chlorine and water. The primary effects of the addition of a low H_2O content can be described by a simplified system of three reactions:

$$\begin{aligned} &(a)\ 2HCl + 1/2O_2 = Cl_2 + H_2O; \\ &(b)\ H_2 + 1/2\ O_2 = H_2O; \\ &(c)\ CO + 1/2O_2 = CO_2. \end{aligned} \qquad (9)$$

This system includes seven compounds, and three equilibrium equations are supplemented by three balances of the fluid components (C, H, O). Because we are interested in the content of elemental chlorine, we will use it as a parameter given by equilibria of Fe chlorides. The equilibrium constants were calculated using the database [9]. The fugacity coefficients of the components were calculated for *PT* experimental conditions using [15]. The initial Cl-free fluid is characterized by CO, CO_2, and H_2O contents controlled by the CCO buffer. As a result of the calculation of the equilibrium state, we acquired correlations of the molar H_2O content and oxygen fugacity as a function of chlorine fugacity (Fig. 5) at three initial H_2O contents.

The thermodynamic calculations showed that the increase in chlorine fugacity in the model fluid is accompanied by an increase in the oxygen fugacity (Fig. 5a). The H_2O content under equilibrium condition strongly decreases with the increase in fCl_2 at an initial H_2O content of <10 mol %, whereas the main Cl part in the system is present in the form of HCl (Fig. 5b). The parameters of the $FeCl_2$–$FeCl_3$ buffer in fCl_2–fO_2 coordinates are intercepted with parameters of the CO_2–CO–H_2O–Cl fluid at an initial H_2O content of <10 mol % (Fig. 5a). Thus, the calculations show that the $FeCl_2$–$FeCl_3$ buffer can determine the chlorine fugacity in both anhydrous and low-H_2O fluid of the CO–CO_2–Cl–H_2O composition. The calculated decrease in H_2O fugacity due to the formation of HCl in our experiments with NaCl is reflected in the absence of sintering of albite glass, which is used as a fluid trap [5]. In a starting glass with ~0.5 wt % of the dissolved and surface-absorbed H_2O, the viscosity of the albite melt is low at $T = 950$°C and $P = 200$ MPa for the formation of a solid mass with entrapped fluid bubble in Cl-free experiments.

Reaction 9a also expresses the chlorine fugacity in pure aqueous fluid with HCl. Figure 2 shows the calculated fCl_2 values for pure aqueous fluid corresponding to 1 M HCl solution, which are a few orders of magnitude lower than in the low-H_2O fluid. The chlorine fugacity increases proportionally to $fO_2^{1/2}$, which is close to the slope of the correlation between the Pt solubility in the brine and oxygen fugacity (Fig. 1). HCl [16] and Cl_2 under its oxidation form in two-phase fluid due to NaCl hydrolysis. The chlorine fugacity in equilibrium (9a) is reverse to the H_2O fugacity, which is lowered in the brine due to the influence of the dissolved salt [17]. Thus, $PtCl_2$ in experiments [6] can also form by the chloration scenario.

According to our experimental data, the active formation of Fe and Cr chlorides can be expected at cumulus parameters of the ultramafic–mafic intrusions. The primary fluid inclusions in quartz [11], which is an accessory mineral of pegmatites of olivine-free rocks (norite, gabbronorite) and anorthosites, and quartz from granophyric inclusions mostly contain NaCl with additions of Ba, K, and Ca chlorides. Only

rare secondary inclusions in healed fractures of olivine of the Stillwater Pt-bearing ultramafic–mafic intrusive (United States) contain Fe chlorides ($FeCl_2$–$FeCl_3$) and Fe and Mn oxychlorides [18]. The rarity of these findings can indicate the difficulty of formation of fluid inclusions in high-temperature low-H_2O fluid conditions.

Our calculations are consistent with the results of [8], which predicted that, at $X_{H2O} < \sim 0.1$, HCl almost replaces H_2O in the fluid, which also does not contain other H-bearing compounds (CH_3Cl, CH_4). Giving the high total Cl content of 10 at % in the initial C–O–H–Cl system, the authors obtained an extremely high Cl_2 content, which, as demonstrated by our experimental data and calculations, is buffered by the reactions with oxides at a lower level. As a result of these reactions at low oxygen fugacity, the fCl_2 values are limited to the maximum possible level for magmatic systems, above which magma is liquated with the formation of the Mg and Fe chloride melt. This fCl_2 level is approximately 3–4 orders of magnitude lower than the level of the $PtCl_2$ stability, which makes it too low for the full transformation of Pt into chloride but is sufficiently high for the formation of $PtCl_2$ in the fluid in equilibrium with the native metal.

SUPPLEMENTARY INFORMATION

The online version contains supplementary material available at https://doi.org/10.1134/S1028334X23603292

ACKNOWLEDGMENTS

We are grateful to Academician L.Ya. Aranovich for constructive criticism that allowed a significant improvement in the initial manuscript. We also acknowledge G.V. Bondarenko for measurement of Raman spectra of some experimental samples at the Institute of Experimental Mineralogy, Russian Academy of Sciences, Chernogolovka, Russia.

FUNDING

This work was supported by the Russian Science Foundation, project no. 23-27-00252.

CONFLICT OF INTEREST

The authors of this work declare that they have no conflicts of interest.

REFERENCES

1. A. G. Mochalov, O. V. Yakubovich, F. M. Stuart, and N. S. Bortnikov, Dokl. Earth Sci. **498** (1), 372–379 (2021). https://doi.org/10.1134/S1028334X2105010X
2. A. E. Boudreau, E. A. Mathez, and I. S. McCallum, J. Petrol. **27** (4), 967–986 (1986). https://doi.org/10.1093/petrology/27.4.967
3. G. P. Orlova, I. D. Ryabchikov, V. V. Distler, and G. D. Gladyshev, Int. Geol. Rev. **29** (3), 360–362 (1987). https://doi.org/10.1080/00206818709466152
4. K. I. Shmulovich, P. G. Bukhtiyarov, and E. S. Persikov, Geochem. Int. **56**, 240–245 (2018). https://doi.org/10.1134/S0016702918030084
5. A. Simakin, T. Salova, A. Y. Borisova, G. S. Pokrovski, O. Shaposhnikova, O. Tyutyunnik, G. Bondarenko, A. Nekrasov, and S. I. Isaenko, Minerals **11**, 225 (2021). https://doi.org/10.3390/min11020225
6. N. A. Sullivan, Z. J. Zajacz, M. Brenan, and A. Tsay, Geochim. Cosmochim. Acta **316**, 253–272 (2022).
7. J. H. Kim and S. I. Woo, Chem. Mater. **10** (11), 3576–3582 (1998). https://doi.org/10.1021/cm980337o
8. E. A. Mathez, V. J. Dietrich, J. R. Holloway, and A. E. Boudreau, J. Petrol. **30** (1), 153–173 (1989). https://doi.org/10.1093/petrology/30.1.153
9. I. Barin, *Thermochemical Data of Pure Substances* (VCH, Weinheim, New York, 1995). https://doi.org/10.1002/978352761982.
10. R. W. Thomas and B. J. Wood, Geochim. Cosmochim. Acta **294**, 28–42 (2021). https://doi.org/10.1016/j.gca.2020.11.018
11. A. E. Boudreau, in *Hydromagmatic Processes and Platinum-Group Element Deposits in Layered Intrusions* (Cambridge Univ. Press, Cambridge, 2019), pp. 101–113.
12. L. Alcaraz, B. Sotillo, J. F. Marco, F. J. Alguacil, P. Fernández, and F. A. López, Materials **14**, 4840 (2021). https://doi.org/10.3390/ma14174840
13. F. Meneses, R. Qi, A. J. Healey, You Yi, I. O. Robertson, S. C. Scholten, A. Keerthi, G. Harrison, L. C. L. Hollenberg, B. Radha, and J.-P. Tetienne, Stray magnetic field imaging of thin exfoliated iron halides flakes (2023). https://doi.org/10.48550/arXiv.2307.10561
14. L. Scholten, C. Schmidt, P. Lecumberri-Sanchez, M. Newville, A. Lanzirotti, M. C. Sirbescu, and M. Steele-MacInnis, Geochim. Cosmochim. Acta **252**, 126–143 (2019). https://doi.org/10.1016/j.gca.2019.03.001
15. S. V. Churakov and M. Gottschalk, Geochim. Cosmochim. Acta **67** (13), 2415–2425 (2003). https://doi.org/10.1016/S0016-7037(02)01348-0
16. N. W. Hanf and M. J. Sole, Trans. Faraday Soc. **66**, 3065–3074 (1970). https://doi.org/10.1039/TF9706603065
17. L. Ya. Aranovich and R. C. Newton, Contrib. Mineral. Petrol. **127**, 261–271 (1997). https://doi.org/10.1007/s004100050279
18. J. J. Hanley, J. E. Mungall, T. Pettke, E. T. C. Spooner, and C. J. Bray, J. Petrol. **49** (6), 1133–1160 (2008). https://doi.org/10.1093/petrology/egn020

Translated by I. Melekestseva